Relation between seepage force and velocity of sand particles during sand boiling

K. Fujisawa[1], A. Murakami[1], S. Nishimura[2] and T. Shuku [2]
[1]*Graduate School of Agriculture, Kyoto University, Kyoto, Japan*
[2]*Graduate School of Environmental and Life Science, Okayama University, Okayama, Japan*
E-mail: fujik@kais.kyoto-u.ac.jp

ABSTRACT: Thus far, the focus of studies on seepage failure, known as sand boiling or the piping phenomenon, has been to determine the critical hydraulic gradient or the critical seepage flow velocity. However, the transport of soil after seepage failure also needs to be well investigated in order to estimate the damage to soil structures or the ground. The purpose of this study is to experimentally investigate the relationship between the seepage force and the velocity of the sand particles during sand boiling induced by upward and horizontal seepage flows. In the experiments, silica sand is used as the test material and the migration velocities of the seepage water and the sand particles are calculated from the measured amounts of their discharge. The test results reveal that the equilibrium of the forces exerted on the sand particles, i.e., gravity, buoyancy and fluid-particle interaction, can be successfully used to estimate the velocity of the sand particles subjected to upward seepage flow and that the seepage force needed for the horizontal transport of the sand tends to decrease as the velocity of the sand particles increases.

1. INTRODUCTION

Sand boiling occurs when soil is subjected to a seepage force greater than one which the soil can resist with its weight. The phenomenon may induce piping beneath or within embankments, such as levees and dams, and can contribute to the failure of or damage to embankments. Foster et al. (2000a, b) statistically investigated the failures of and accidents to world-wide embankment dams, and reported that piping accounted for approximately 40% of them. Rechards & Reddy (2007) summarized a series of problems concerning piping and provided case histories of piping dam failures. There are plenty of aging small embankment dams for irrigation in a variety of regions in Japan. These small dams often suffer from water leakage, which may be induced by the piping phenomenon. Piping is a serious problem for these embankments, because it develops insidiously, and sand boiling is a key mechanism which causes the fluidization and the relocation of sandy soil.

Piping is both an old and a new research topic on which numerous studies have been based (e.g., Tanaka, *et al*., 1982; Sellmeijer, 1988; Sellmeijer & Koenders, 1991; Meyer, *et al*., 1994; Skempton & Brogan, 1994; Tanaka & Verruijt, 1999; Ojha, *et al*., 2003; Shamy & Aydin, 2008; Rechards & Reddy, 2012; Zhou, *et al*., 2012). Most of the previous studies have focused on determining the critical values of the hydraulic gradients, the seepage velocities and the hydraulic heads (e.g., Lambe & Whitman, 1979; Tanaka, *et al*., 1982; Sellmeijer, 1988; Meyer, *et al*., 1994; Skempton & Brogan, 1994; Tanaka & Verruijt, 1999; Ojha, *et al*., 2003). Skempton & Brogan (1994) first showed that the internal instability of soil decreased its resistibility against piping and that the critical hydraulic gradient became smaller than that of the internally stable soil. Ojha, *et a*l. (2003) proposed two models for predicting the critical head at the initiation of levee piping and compared their performance with that of existing models. Richards & Reddy (2007) described the progress of the criteria for the critical values in their review paper and it has great references.

The criteria for critical hydraulic gradients, seepage velocities and hydraulic heads can predict whether or not sand boiling or piping occurs. However, the criteria cannot predict how the boiling or piping develops, such as the speed and the direction of the piping. This implies that the extent of the damage to the soil structures due to piping cannot be assessed even if the existence or the non-existence can be judged. The maintenance of levees and embankment dams is becoming more and more important; this necessitates accurate estimates of the extent of the embankment damage. To this end, the present study focuses on the phenomenon of sand boiling and investigates how much and how fast the sand particles are transported by the seepage flow, because these are fundamental issues in estimating the extent of damage due to piping. If the speed of the migrating sand particles is obtained, it helps to know how much soil may be washed out during a flooding event.

This paper, at the beginning, refers to the force exerted on the sand particles by the seepage flow, the so-called seepage force, formulated from macroscopic and microscopic points of view. Then, an experimental investigation of the velocities of the sand particles transported by upward and horizontal seepage flows is presented via two types of experiments, in which the migration velocity of the sand particles is obtained, as well as the seepage flow velocity and the pore water pressure, from the measurement of their discharge rates. The experimental results reveal the relationship between the seepage force and the velocity of the transported sand particles. This paper shows that the velocity of the sand particles during sand boiling, due to the upward seepage flow, can be well estimated by the equilibrium of the forces induced by the pore water pressure, the seepage flow velocity and the gravity, and that the seepage force needed for the horizontal transport of the sand tends to decrease as the velocity of the sand particles increases.

2. SEEPAGE FORCE

2.1 Macroscopic and microscopic water pressure

Seepage force is defined as the force exerted on a sand mass of unit volume by the seepage flow. Figure 1 illustrates the microscopic domain of sand covered with seepage water. As shown, the sand particles have normal and tangential stress on their surfaces. The normal stress is the pore water pressure and the tangential stress comes from the friction between the flowing seepage water and the sand particles. Note that the microscopic water pressure exerted on each particle surface differs from that measured by piezometers. The former is the local microscopic pressure, while the latter is the average macroscopic pressure. It is quite difficult to measure the microscopic quantities, and the force applied to each particle cannot be determined. However, by measuring the macroscopic quantities, the seepage force applied to the sand can be estimated. To understand the relationship between microscopic and macroscopic forces on the interaction between the seepage water and the sand particles, macroscopic coordinate $\boldsymbol{X}$, which describes the average quantities, and microscopic coordinate $\boldsymbol{y}$, which describes the local quantities, are introduced here. Macroscopic coordinate $\boldsymbol{X}$ is used to deal with average quantities and it has a rough resolution. The scale for macroscopic coordinate $\boldsymbol{X}$ is so large that it cannot recognize the local quantities. Microscopic coordinate $\boldsymbol{y}$ is defined at a given point of macroscopic coordinate $\boldsymbol{X}$ shown in Figure 1. Since it has a high resolution and sufficiently fine scales, it can treat the changes in local quantities which cannot be seen in macroscopic coordinate $\boldsymbol{X}$. Using these two coordinate systems, a local quantity φ is expressed

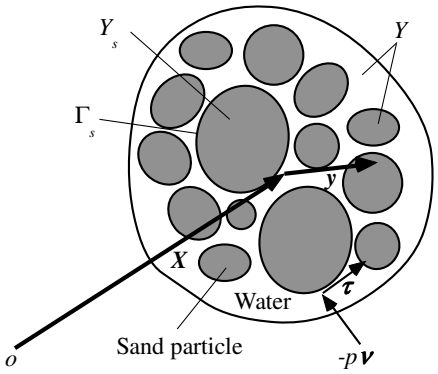

Figure 1 Sand particles subjected to upward seepage flow (Microscopic domain)

as $\varphi(\boldsymbol{X},\boldsymbol{y})$. The average $\overline{\varphi}$ is obtained by volume averaging.

$$\overline{\varphi}(\boldsymbol{X}) = \frac{1}{V_y}\int_Y \varphi(\boldsymbol{X},\boldsymbol{y})\, dV_y \tag{1}$$

where Y and V_y denote the microscopic domain around a given macroscopic point $\boldsymbol{X}$ and the volume in the domain, respectively. It should be noted that the average quantity $\overline{\varphi}$ becomes a function of only $\boldsymbol{X}$, as seen in Eq. (1), because $\varphi(\boldsymbol{X},\boldsymbol{y})$ has been integrated with respect to $\boldsymbol{y}$. Since macroscopic coordinate $\boldsymbol{X}$ must be equivalent to the average local point $\boldsymbol{X}$+$\boldsymbol{y}$ (See Figure 1), the following relationship is derived:

$$\boldsymbol{X} = \frac{1}{V_y}\int_Y \boldsymbol{X}+\boldsymbol{y}\, dV_y \tag{2}$$

Eq. (2) can be reduced to the following equation:

$$\int_Y \boldsymbol{y}\, dV_y = \boldsymbol{0} \tag{3}$$

which means that macroscopic coordinate $\boldsymbol{X}$ corresponds to the centroid of microscopic domain Y surrounding the point $\boldsymbol{X}$. The pore water pressure can be measured as the average value at the measuring point, which can be denoted as $\overline{p}(\boldsymbol{X})$. The gradient of the measured pore water pressure is also a function of macroscopic coordinate X and it can be written by $\partial\overline{p}(\boldsymbol{X})/\partial\boldsymbol{X}$. With $\overline{p}(\boldsymbol{X})$ and $\partial\overline{p}(\boldsymbol{X})/\partial\boldsymbol{X}$, the local pore water pressure, $p(\boldsymbol{X},\boldsymbol{y})$, is described as

$$p(\boldsymbol{X},\boldsymbol{y}) = \overline{p}(\boldsymbol{X}) + \frac{\partial\overline{p}(\boldsymbol{X})}{\partial\boldsymbol{X}}\boldsymbol{y} + p^*(\boldsymbol{X},\boldsymbol{y}) \tag{4}$$

where $p^*(\boldsymbol{X},\boldsymbol{y})$ denotes the deviation from the linear estimation by average pore water pressure $\overline{p}(\boldsymbol{X})$ and its gradient $\partial\overline{p}(\boldsymbol{X})/\partial\boldsymbol{X}$. For example, on the particle surfaces where the seepage water approaches, the water pressure microscopically increases, while on the particle surfaces where the seepage water gets away, the pressure microscopically deceases. The deviation term $p^*(\boldsymbol{X},\boldsymbol{y})$ includes such microscopic variations which cannot be described by the macroscopic quantities. Taking into account that the macroscopic quantities are the volume average of the microscopic ones, the following equations for the pore water pressure and its gradient must be satisfied:

$$\overline{p}(\boldsymbol{X}) = \frac{1}{V_y}\int_Y p(\boldsymbol{X},\boldsymbol{y})\, dV_y \tag{5a}$$

$$\frac{\partial\overline{p}(\boldsymbol{X})}{\partial\boldsymbol{X}} = \frac{1}{V_y}\int_Y \frac{\partial p(\boldsymbol{X},\boldsymbol{y})}{\partial\boldsymbol{y}}\, dV_y \tag{5b}$$

Substituting Eq. (4) into Eqs. (5a) and (5b), the following relations for $p^*(\boldsymbol{X},\boldsymbol{y})$ are derived with the aid of Eq. (3):

$$\int_Y p^*(\boldsymbol{X},\boldsymbol{y})\, dV_y = 0 \tag{6a}$$

$$\int_Y \frac{\partial p^*(\boldsymbol{X},\boldsymbol{y})}{\partial\boldsymbol{y}}\, dV_y = 0 \tag{6b}$$

2.2 Averaging microscopic water pressure and friction

Since seepage force $\boldsymbol{f}$ is a macroscopic quantity, defined as the total force exerted on sand of unit volume by seepage water, it is written using the following equation:

$$\boldsymbol{f}(\boldsymbol{X}) = \frac{1}{V_y}\int_{\Gamma_s} -p(\boldsymbol{X},\boldsymbol{y})\boldsymbol{\nu}\, dS_y + \frac{1}{V_y}\int_{\Gamma_s} \boldsymbol{\tau}(\boldsymbol{X},\boldsymbol{y})\, dS_y \tag{7}$$

where $\boldsymbol{\nu}$ and $\boldsymbol{\tau}$ are the unit normal outward vector on the sand particle faces and the friction stress vector, respectively, Γ_s denotes the surfaces of the sand particles and S_y means the surface area, as shown in Figure 1. Using Eq. (4), the first term on the right-hand side of Eq. (7) can be broken down as follows:

$$\begin{aligned}
\frac{1}{V_y}\int_{\Gamma_s} -p\boldsymbol{\nu}\, dS_y &= \frac{1}{V_y}\int_{\Gamma_s} -(\overline{p} + \frac{\partial\overline{p}}{\partial\boldsymbol{X}}\boldsymbol{y} + p^*)\boldsymbol{\nu}\, dS_y \\
&= \frac{1}{V_y}\int_{Y_s} -\frac{\partial}{\partial\boldsymbol{y}}\left(\overline{p} + \frac{\partial\overline{p}}{\partial\boldsymbol{X}}\boldsymbol{y}\right) dV_y + \frac{1}{V_y}\int_{\Gamma_s} -p^*\boldsymbol{\nu}\, dS_y \\
&= \frac{1}{V_y}\int_{Y_s} -\frac{\partial\overline{p}}{\partial\boldsymbol{X}} dV_y + \frac{1}{V_y}\int_{\Gamma_s} -p^*\boldsymbol{\nu}\, dS_y \\
&= -\frac{\partial\overline{p}}{\partial\boldsymbol{X}}\frac{1}{V_y}\int_{Y_s} dV_y + \frac{1}{V_y}\int_{\Gamma_s} -p^*\boldsymbol{\nu}\, dS_y \\
&= -(1-n)\frac{\partial\overline{p}}{\partial\boldsymbol{X}} + \frac{1}{V_y}\int_{\Gamma_s} -p^*\boldsymbol{\nu}\, dS_y
\end{aligned} \tag{8}$$

where Y_s denotes the domain of the sand particles (the domain does not include the voids (See Figure 1)) and n denotes the porosity as a macroscopic quantity. In the second equality of Eq. (8), the divergence theorem of Gauss was applied over microscopic coordinate $\boldsymbol{y}$, and the fact that the volume of the particle domain is $(1-n)V_y$ was taken into account in the last equality. It is worth noting that the integrals conducted in Eq. (8) are all for microscopic coordinate $\boldsymbol{y}$ and do not operate the macroscopic quantities because they are the functions of macroscopic coordinate $\boldsymbol{X}$. Substituting Eq. (8) into Eq. (7), the seepage force is rewritten in the following form:

$$\boldsymbol{f} = -(1-n)\frac{\partial\overline{p}}{\partial\boldsymbol{X}} + \frac{1}{V_y}\left(\int_{\Gamma_s} -p^*\boldsymbol{\nu}\, dS_y + \int_{\Gamma_s} \boldsymbol{\tau}\, dS_y\right) \tag{9}$$

The second term on the right-hand side of Eq. (9) cannot be measured directly; the term is modelled with the average velocity of the seepage water and the hydraulic conductivity, as explained in the next section.

2.3 Relation of seepage force and hydraulic conductivity

Figure 2 shows a microscopic illustration of the seepage water steadily flowing through the sand particles. The reason the steady state of the seepage flow is considered here is that the coefficient of hydraulic conductivity is the physical quantity assuming the steady state of the seepage flow. The forces applied to the seepage water are balanced under its steady state, described by the following equation:

$$\int_{\Gamma_w} -p\boldsymbol{\nu}'\, dS_y + \int_{\Gamma_s} -p\boldsymbol{\nu}'\, dS_y + \int_{\Gamma_s} \boldsymbol{\tau}'\, dS_y + \int_{Y_w} \rho_w\boldsymbol{g}\, dV_y = \boldsymbol{0} \tag{10}$$

where Y_w, Γ_w, $\boldsymbol{g}$, $\boldsymbol{\nu}'$ and $\boldsymbol{\tau}'$ denote the domain of the voids filled with the seepage water, the boundary of the microscopic domain, the vector of the gravitational acceleration, the unit normal outward vector of the seepage water domain and the friction stress exerted to the seepage water from the particle faces, respectively (See Figure 2). Note that $\boldsymbol{\nu}$ and $\boldsymbol{\tau}$ in Eq. (7) are the unit normal outward vector and the friction stress of the sand particles, respectively, and that they have the following relation with $\boldsymbol{\nu}'$ and $\boldsymbol{\tau}'$ in Eq. (10):

$$\boldsymbol{\nu}' = -\boldsymbol{\nu} \tag{11a}$$

$$\boldsymbol{\tau}' = -\boldsymbol{\tau} \tag{11b}$$

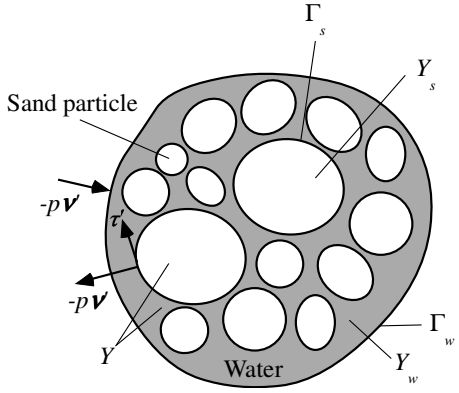

Figure 2 Forces exerted on steadily flowing seepage water (Microscopic domain)

The first term on the left-hand side of Eq. (10) is the resultant force due to the water pressure applied to the seepage water itself, while the second and third terms are attributed to the reactive pressure and the friction from the sand particles, respectively, and the last tem results from the body force due to gravity. Substituting Eq. (4) into Eq. (10), it can be broken down as follows:

$$\int_{\Gamma} -\left(\overline{p}(\boldsymbol{X}) + \frac{\partial \overline{p}}{\partial \boldsymbol{X}}\boldsymbol{y}\right)\boldsymbol{\nu}'\, dS_y + \int_{\Gamma_w} -p^*\boldsymbol{\nu}'\, dS_y + \int_{\Gamma_s} -p^*\boldsymbol{\nu}'\, dS_y + \int_{\Gamma_s} \boldsymbol{\tau}'\, dS_y + \int_{Y_w} \rho_w \boldsymbol{g}\, dV_y = \boldsymbol{0}\ ,\ \Gamma \equiv \Gamma_s \cup \Gamma_w$$

$$\Rightarrow \int_{Y_w} -\frac{\partial \overline{p}}{\partial \boldsymbol{X}}\, dV_y - \int_Y \frac{\partial p^*}{\partial \boldsymbol{y}} dV_y + \int_{\Gamma_s} -p^*\boldsymbol{\nu}'\, dS_y + \int_{\Gamma_s} \boldsymbol{\tau}'\, dS_y + \int_{Y_w} \rho_w \boldsymbol{g}\, dV_y = \boldsymbol{0}$$

$$\Rightarrow -nV_y \frac{\partial \overline{p}}{\partial \boldsymbol{X}} + \int_{\Gamma_s} -p^*\boldsymbol{\nu}'\, dS_y + \int_{\Gamma_s} \boldsymbol{\tau}'\, dS_y + nV_y \rho_w \boldsymbol{g} = \boldsymbol{0}$$

$$\left(\because \int_Y \frac{\partial p^*}{\partial \boldsymbol{y}} dV_y = 0 \text{ from Eq. (5b)},\ \int_{Y_w} dV_y = nV_y\right)$$

$$\Rightarrow n\left(-\frac{\partial \overline{p}}{\partial \boldsymbol{X}} + \rho_w \boldsymbol{g}\right) = \frac{1}{V_y}\left(\int_{\Gamma_s} -p^*\boldsymbol{\nu}\, dS_y + \int_{\Gamma_s} \boldsymbol{\tau}\, dS_y\right)$$

$$\left(\because \boldsymbol{\tau}' = -\boldsymbol{\tau}\ ,\ \boldsymbol{\nu}' = -\boldsymbol{\nu} \text{ from Eq. (11)}\right) \tag{12}$$

Since Darcy's law is given by

$$\overline{\boldsymbol{v}}_w = -\frac{k}{\rho_w g}\left(\frac{\partial \overline{p}}{\partial \boldsymbol{X}} - \rho_w \boldsymbol{g}\right) \tag{13}$$

where $\overline{\boldsymbol{v}}_w$ is the volume-averaged velocity of the seepage water flowing through the particle-to-particle interspace, known as the Darcy velocity. Hence, the relationship between the Darcy velocity and the microscopic seepage velocity, $\boldsymbol{v}_w(\boldsymbol{X}, \boldsymbol{y})$, is

$$\overline{\boldsymbol{v}}_w(\boldsymbol{X}) = \frac{1}{V_y}\int_Y \boldsymbol{v}_w(\boldsymbol{X}, \boldsymbol{y})\, dV_y \tag{14}$$

Substituting Eq. (14) into the left-hand side of Eq. (12), yields

$$\frac{n\rho_w g}{k}\overline{\boldsymbol{v}}_w = \frac{1}{V_y}\left(\int_{\Gamma_s} -p^*\boldsymbol{\nu}\, dS_y + \int_{\Gamma_s} \boldsymbol{\tau}\, dS_y\right) \tag{15}$$

Using the relationship in Eq. (15), Eq. (9) is reduced to

$$\boldsymbol{f} = -(1-n)\frac{\partial \overline{p}}{\partial \boldsymbol{X}} + \frac{n\rho_w g}{k}\overline{\boldsymbol{v}}_w \tag{16}$$

which shows that the seepage force can be obtained from the macroscopic quantities. For a later discussion, the phase average velocity of the seepage flow is adopted instead of the Darcy velocity.

$$\tilde{\boldsymbol{v}}_w(\boldsymbol{X}) \equiv \frac{1}{V_w}\int_{Y_w} \boldsymbol{v}_w(\boldsymbol{X}, \boldsymbol{y})\, dV_y = \frac{1}{nV_y}\int_Y \boldsymbol{v}_w(\boldsymbol{X}, \boldsymbol{y})\, dV_y$$

$$\left(\because \boldsymbol{v}_w(\boldsymbol{X}, \boldsymbol{y}) = 0 \text{ in } Y_s, \text{ and } V_w = nV_y\right) \tag{17}$$

where $\tilde{\boldsymbol{v}}_w$ and V_w denote the phase average velocity and the volume of the water phase, respectively. The difference between the volume average and the phase average is that the former averaging is conducted for the entire volume of the microscopic domain, as has been shown in Eq. (1), but the latter averaging operates only for the water phase, as seen in Eq. (17). Comparing Eq. (14) with Eq. (17), the following relationship between the volume average velocity and the phase average velocity is obtained:

$$\overline{\boldsymbol{v}}_w = n\tilde{\boldsymbol{v}}_w \tag{18}$$

If the phase average velocity is adopted for estimating the seepage force, Eq. (16) is presented as follows:

$$\boldsymbol{f} = -(1-n)\frac{\partial \overline{p}}{\partial \boldsymbol{X}} + \frac{n^2\rho_w g}{k}\tilde{\boldsymbol{v}}_w \tag{19}$$

In this paper, Eq. (19) is mainly used to consider the seepage force driving the sand particles. At the end of this chapter, a definition for the phase average velocity of the sand particles is given in order to consider their migration due to the seepage flow.

$$\tilde{\boldsymbol{v}}_s(\boldsymbol{X}) \equiv \frac{1}{V_s}\int_{Y_w} \boldsymbol{v}_s(\boldsymbol{X}, \boldsymbol{y})\, dV_y = \frac{1}{(1-n)V_y}\int_Y \boldsymbol{v}_s(\boldsymbol{X}, \boldsymbol{y})\, dV_y$$

$$\left(\because \boldsymbol{v}_s(\boldsymbol{X}, \boldsymbol{y}) = 0 \text{ in } Y_w, \text{ and } V_s = (1-n)V_y\right) \tag{20}$$

where $\boldsymbol{v}_s$, $\tilde{\boldsymbol{v}}_s$ and V_s denote the local and the phase average velocity of the sand particles and the volume of the water phase, respectively.

3. SAND BOIL TESTS BY UPWARD SEEPAGE FLOW

3.1 Test apparatus and materials

To measure the migration velocity of the sand particles during sand boiling, the test apparatus shown in Figure 3, with a U-shaped acrylic cylinder, was developed. The acrylic cylinder was transparent and had a thickness of 5 mm and an inner diameter of 80 mm. Its length and width are shown in Figure 3. Silica sands #5 and #6 were adopted as the test materials. The particle sizes and the densities of these two sands are listed in Table 1. The sand boil tests reported in this paper allow the sand particles to spill out of the cylinder. Therefore, a U-shaped cylinder was used, which enabled the sand located upstream in it to be naturally supplied when the migration of the sand particles started. The upstream end of the cylinder was connected to a water tank with a hose, which was filled with water at a constant level. By adjusting the height of the water tank, the hydraulic gradient within the cylinder was changed. A smooth plastic glide, with an angle of nearly 45 degrees, was attached to the downstream end, which conveyed the discharging

water and the sand particles to a vessel, i.e., Vessel 1 in Figure 3, located right beside the cylinder. It was confirmed that the plastic slope was smooth and steep enough to convey the discharging sand particles without their suspension on the slope. The three piezometers were installed at the vertical part of the downstream cylinder and the hydraulic heads and gradients were measured by manometers.

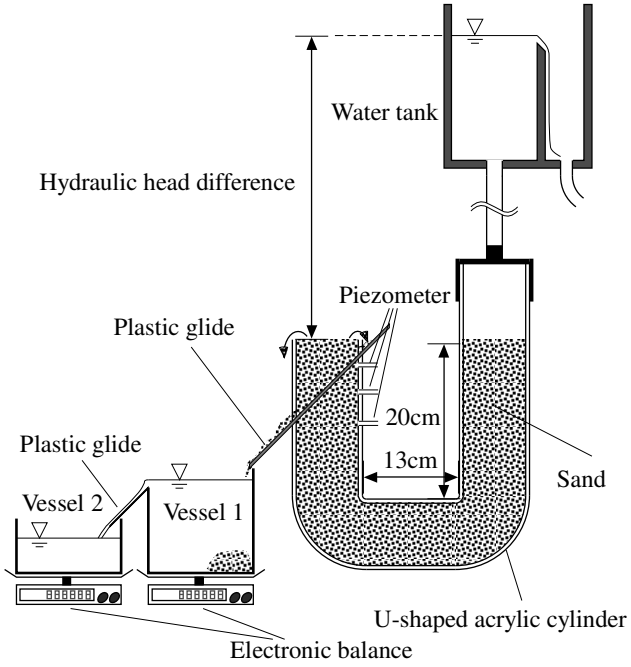

Figure 3 Test apparatus with U-shaped acrylic cylinder

Table 1 Particle sizes and densities of test materials

Silica sand	#5	#6
Grain diameter [mm]	0.3-0.8	0.2-0.4
Mean diameter [mm]	0.58	0.32
Grain density [g/cm^3]	2.65	2.63
Min. density [g/cm^3]	1.30	1.25
Max. density [g/cm^3]	1.55	1.50
Min. void ratio	0.70	0.75
Max. void ratio	1.03	1.10

The effluent from the cylinder was the mixture of the seepage water and the moving sand particles. The discharging mixture first entered Vessel 1, as shown in Figure 3. Since the vessel consistently reserved water at its full capacity, water of the same volume as the effluent flowed out of Vessel 1 and into Vessel 2, as seen in Figure 3. The sand particles, discharged from the cylinder, settled in Vessel 1 and the equivalent amount of water was replaced with the sand particles.

Assuming that the seepage water of a volume ΔV_w and the sand particles of a volume ΔV_s were discharged from the cylinder during a certain interval Δt, the water in Vessel 1 is replaced with the sand particles at a volume of ΔV_s. Hence, the weight of Vessel 1 increases by the following amount:

$$\Delta W_1 = (\rho_s - \rho_w) g \Delta V_s \tag{21}$$

where ΔW_1 and ρ_s denote the weight increment of Vessel 1 and the density of the sand particles, respectively. Then, the water of volume $\Delta V_w + \Delta V_s$ enters Vessel 2 from Vessel 1 and the weight of Vessel 2 increases by the following amount:

$$\Delta W_2 = \rho_w g (\Delta V_s + \Delta V_w) \tag{22}$$

where ΔW_2 denotes the weight increment of Vessel 2. The volumes of ΔV_w and ΔV_s are calculated from Eqs. (21) and (22) as

$$\Delta V_s = \frac{\Delta W_1}{(\rho_s - \rho_w) g} \tag{23a}$$

$$\Delta V_w = \frac{\Delta W_2}{\rho_w g} - \frac{\Delta W_1}{(\rho_s - \rho_w) g} \tag{23b}$$

which means that the volumes of the discharged water and the sand particles can be separately measured. In the tests, the weights of Vessels 1 and 2 were measured by electric balances and the data were transferred to a laptop computer and recorded every second.

3.2 Preparation and procedures

Before the sand boil tests, the U-shaped acrylic cylinder was filled with the test materials, as shown in Figure 3. The deaerated water was poured into the cylinder and then either Silica sand #5 or #6 was poured slowly into the water. After some amount of sand had accumulated in the cylinder, the sand face was hit with a tamping bar several times to pack the sand. This was repeated until the sand was filled to the predetermined height. The dry density of the sand in the cylinder was calculated from the volume of the sand region (3,684 cm^3), measured before the tests, and the dry weight of the sand put into the cylinder. This dry density was the average density in the cylinder.

After the cylinder was filled up with the sand, the upstream end of the cylinder was connected to the water tank with a hose, and a difference in hydraulic head of nearly 40 cm was given to make the seepage water flow. After the steady seepage flow was confirmed, the hydraulic conductivity was measured; the discharging rate of the effluent water from the cylinder was easily obtained from the weight of Vessel 2. The hydraulic conductivity measured at this stage, before sand boiling, is called the initial hydraulic conductivity in this paper.

Following the measurement of the initial hydraulic conductivity, the water tank was gradually lifted up and the hydraulic gradient within the cylinder was increased. When the hydraulic gradient approached the critical value, the sand particles at the downstream cylinder began to discharge slightly. The discharge of the sand particles was often observed on the interior side of the outlet where the seepage length was shorter. Then, the water tank was fixed at a constant level and the hydraulic conductivity was measured again to confirm the initiation of sand boiling, which is called the hydraulic conductivity at sand boil hereafter in this paper.

Finishing the remeasurement of the hydraulic conductivity, the water tank was lifted up again, by about 5cm, to induce sand boiling and the discharge of the sand from the whole area of the outlet. It was visually confirmed that the sand particles moved almost uniformly at the cross-section and that the boiling did not concentrate to a specific region. Then, the water tank was fixed again and the measurement of the discharging rate of the sand particles was started. According to Eq. (23), the volume increments of the discharged water and sand particles were obtained. The phase average velocities of the seepage water and the sand particles were estimated as follows:

$$\tilde{v}_{w,z} = \frac{\Delta V_w}{n A \Delta t} \tag{24a}$$

$$\tilde{v}_{s,z} = \frac{\Delta V_s}{(1-n) A \Delta t} \tag{24b}$$

where $\tilde{v}_{w,z}$ and $\tilde{v}_{s,z}$ denote the vertical and the upward components.

Starting the discharge of the sand particles, the top face of the sand filled in the upstream cylinder (the right vertical cylinder in Figure 3) slowly sank as is dragged into the upstream curve (the right bend of the cylinder in Figure 3). When the sand face reached

the upstream bend, sand boiling explosively occurred and most of the sand rapidly flowed out. The migration velocity of the sand particles in this final stage was so quick that it could not be stably measured. Therefore, it should be noted that the sand boil tests reported in this paper investigated the relatively slow velocity of the sand particles up to the final stage.

3.3 Results and discussions

For the purpose of measuring the velocities of the sand particles during sand boiling, the sand boil tests were carried out four times for each test material. Table 2 lists porosity n, relative density D_r, initial hydraulic conductivity k_0, hydraulic conductivity at sand boil k and water temperature T for all the tests. In the table, the values of the hydraulic conductivities enclosed in parentheses means those translated at 15 degrees centigrade.

Taking Test no. U4 as an example, the typical results are explained here. Figure 4 shows the temporal alterations of vertical velocities $\tilde{v}_{w,z}$ and $\tilde{v}_{s,z}$ during sand boiling. These velocities were calculated from Eq. (24), and Δt in the equation was placed in the range of 3 to 10 seconds depending on the discharge rates of the seepage water and the sand particles (The greater the discharge rates became, the shorter time intervals were taken). As shown in Figure 4, the sand particle velocity was slight up to 100 seconds after the sand boil was initiated, and then it sharply increased. The velocity accelerated to approximately 1.5 cm/s, as seen in Figure 4. The temporal change in the hydraulic gradient, while the sand particles were discharging, is shown by Figure 5, where the vertical axis of $-dh/dz$ denotes the absolute value of the hydraulic gradient. The figure indicates that the hydraulic gradient notably decreased when the discharge of the sand particles was rapid. The reason is inferred to be that the migration of the sand particles in the downstream cylinder needed a lower hydraulic gradient than that in the other parts.

Using the velocities of the seepage water, the sand particles and the hydraulic gradient, which are shown in Figures 4 and 5, the seepage force acting on the sand can be estimated. Translating the phase average velocity of the seepage water in Eq. (19) into the relative velocity from the sand particles, the vertical component of the seepage force can be written in the following form:

$$f_z = -(1-n)\frac{\partial \overline{p}}{\partial z} + \frac{n^2 \rho_w g}{k}(\tilde{v}_{w,z} - \tilde{v}_{s,z}) \tag{25}$$

where f_z and z denotes the vertical component of the seepage force and the vertical axis for macroscopic quantities, respectively. Figure 6 shows the temporal change in the seepage force calculated by Eq. (25) during sand boiling. For the calculation, the values of the velocities of the seepage water, the sand particles and the hydraulic gradient were given by the data shown in Figures 4 and 5. The hydraulic conductivity at sand boil and the porosity were assumed to have the values shown in Table 2. As shown in Figure 6, the seepage force was kept constant even when the sand particles were moving upward, although the data fluctuated at the end. This fluctuation was induced by the waves of the water surface in Vessels 1 and 2 shown in Figure 3, because the water surface became wavy and the output values of the electric balances were slightly disturbed when the discharge of the water and the sand increased.

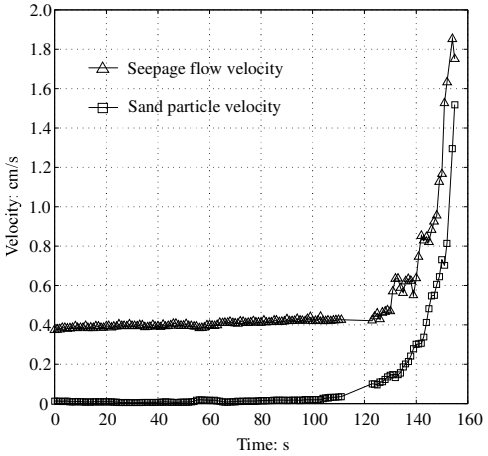

Figure 4 Upward velocities of sand and seepage water during sand boiling in Test no. U4

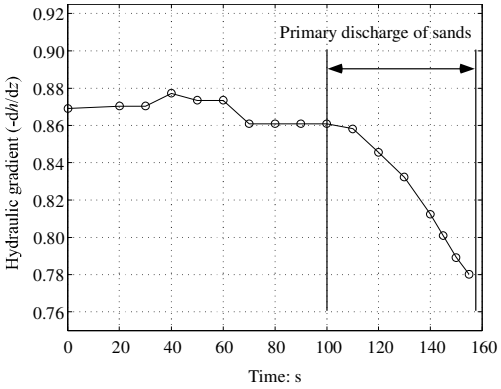

Figure 5 Temporal change in hydraulic gradient during sand boiling

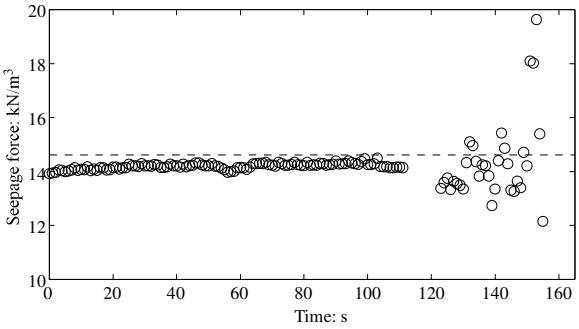

Figure 6 Relationship between seepage force and elapsed time

Table 2 Porosity, density and hydraulic conductivity in sand boil tests with U-shaped cylinder

Test no.	Silica sand	Porosity n	Relative density D_r [%]	Temperature T [deg. C]	Initial hydraulic conductivity k_0 [cm/s]	Hydraulic conductivity at sand boil k [cm/s]
U1	#5	0.440	75.2	7.0	0.105 (0.132)	0.155 (0.195)
U2		0.435	80.0	7.0	0.108 (0.136)	0.126 (0.158)
U3		0.434	80.9	6.8	0.0989 (0.124)	0.199 (0.250)
U4		0.437	78.1	14.2	0.113 (0.116)	0.187 (0.192)
U5	#6	0.449	66.3	9.4	0.0728 (0.0861)	0.066 (0.078)
U6		0.444	71.3	12.5	0.0733 (0.0774)	0.071 (0.075)
U7		0.443	72.3	5.6	0.0721 (0.0934)	0.107 (0.130)
U8		0.446	69.3	7.6	0.0848 (0.103)	0.103 (0.125)

The dashed line means the value of the gravity exerted on the soil particles within the sand of a unit volume, i.e., $(1-n)\rho_s g$, which is significantly close to the values of the seepage force. This fact implies that the seepage force given by Eq. (25) is equilibrated with the weight of the sand particles within a unit volume of the sand and revealed that Eq. (25) is applicable to estimating the seepage force when the sand particles are in motion.

From this fact, the following equilibrium equation between the seepage force and the weight of the sand particles within a unit volume can be derived:

$$(1-n)\rho_s g = -(1-n)\frac{\partial \overline{p}}{\partial z} + \frac{n^2 \rho_w g}{k}(\tilde{v}_{w,z} - \tilde{v}_{s,z}) \tag{26}$$

Solving Eq. (26) for the phase average velocity of the sand particles, it can be reduced to

$$\tilde{v}_{s,z} = \tilde{v}_{w,z} - \frac{k(1-n)}{n^2}\left(\frac{\rho_s}{\rho_w} + \frac{1}{\rho_w g}\frac{\partial \overline{p}}{\partial z}\right) \tag{27}$$

which suggests that sand particle velocity $\tilde{v}_{s,z}$, transported by the seepage flow, is predictable. Figure 7 shows the relationship between the measured and the predicted velocities of the sand particles in Test no. U4, in which the horizontal axis corresponds to the measured velocities shown in Figure 4 and the vertical axis presents the estimated velocities calculated from Eq. (27). As seen in the figure, the measured and the estimated values agree well with each other.

Figure 8 compiles the relationship between the measured and the estimated velocities of the sand particles obtained from all the tests using Silica sand #5 (Test nos. U1 to U4). As shown in Figure 8, the data points are distributed around the line, passing the origin and having the unit gradient, and the measured velocities of the sand particles are in notably good agreement with the estimated ones when the values are within 0 to 0.8 cm/s.

Figure 9 shows a similar relationship to Figure 8, obtained from the results of Test nos. U5 to U8 using Silica sand #6. Although the data points in the figure seem to be scattered compared with Figure 8, they are also distributed along the central line. These results have shown that the velocities of the sand particles transported by the upward seepage flow are predictable in the manner described by Eq. (27).

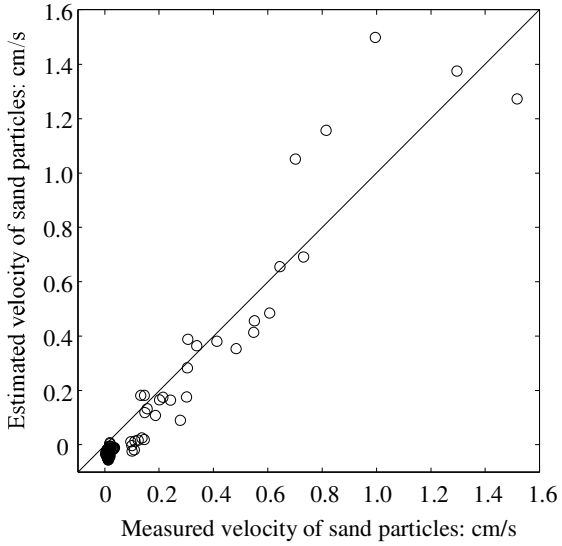

Figure 7 Relationship between measured and estimated values of sand particle velocity

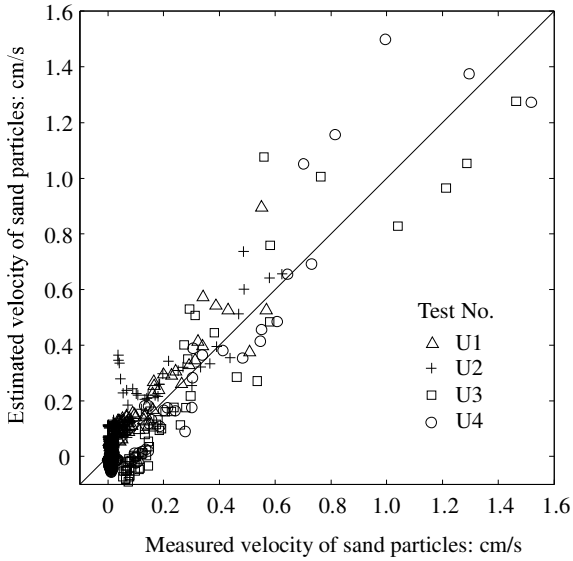

Figure 8 Measured and estimated values of sand particle velocity (Silica sand #5)

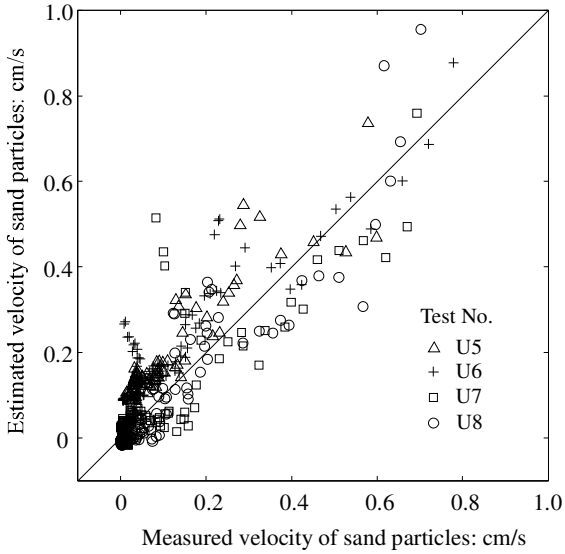

Figure 9 Measured and estimated values of sand particle velocity (Silica sand #6)

4. TRANSPORT OF SAND PARTICLES BY HORIZONTAL SEEPAGE FLOW

In the previous section, the relationship between the seepage force and the velocity of the sand particles transported by the upward seepage flow has been investigated. Unlike the upward migration of the sand particles, the friction force between the sand and the walls is significant when the sand particles are transported in the horizontal direction, and the seepage force greater than the friction force is necessary to induce the horizontal transport of the sand. Herein, the relationship between the seepage force and the velocity of the sand particles transported horizontally is investigated.

4.1 Test apparatus and procedures

Figure 10 shows the test apparatus for the investigation of the relationship between the seepage force and the velocity of the sand particles horizontally transported by seepage flow. The apparatus is quite similar to that in Figure 3. The only difference is in the shape of the cylinder including the test materials. A horizontal acrylic pipe is used instead of the U-shaped cylinder shown in Figure 3. The pipe was transparent and had a length of 100 cm and a diameter of 5.2 cm. Three piezometers were attached near its outlet. The test materials are Silica sands #5 and #6, and the test procedure is also similar to that mentioned in the previous chapter. After the pipe was filled with either of the test materials and deaerated water, the seepage flow was induced by lifting up the water tank and the

Conductivity was measured under a steady condition. The measurement was conducted at a relatively high water level before the sand particles started to move. After that, the water tank was elevated by about 15 cm to cause the migration of the sand particles, due to the horizontal seepage flow, and the discharge rates of the seepage water and the sand particles began to be measured. The measurement procedure was the same as that mentioned in the previous chapter.

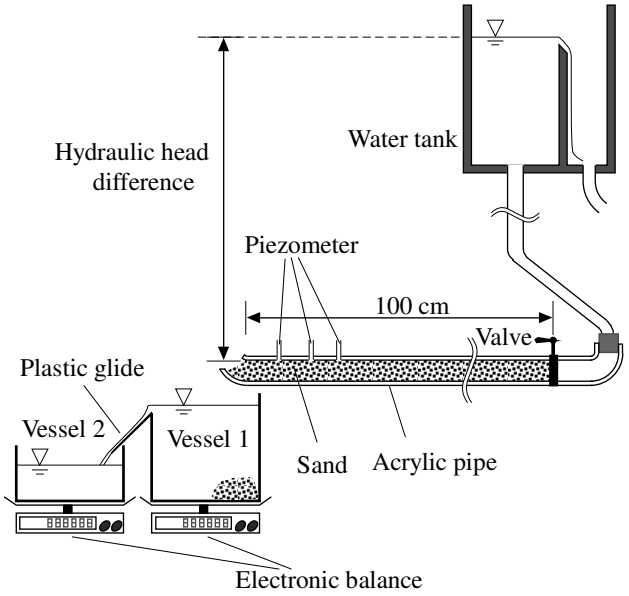

Figure 10 Test apparatus for horizontal migration of sands

4.2 Results and discussions

The tests were carried out four times for each test material. Porosity n, relative density D_r, temperature T and hydraulic conductivity k for each test are listed in Table 3. Taking Test no. H6 as an example, the typical results are explained below.

Figure 11 shows the temporal change in the seepage velocity and the sand particle velocity. As seen in the figure, the velocity of the sand particles was very slow up to 100 seconds after the water tank was lifted up. Then, the velocity started to rapidly increase and fluctuate around 130 seconds. Figure 12 shows pictures of the sand transport during Test no. H6. Only the upper part of the sand filling the pipe was moving up to 120 seconds, as shown in Figure 12(a), so that the measured velocity did not stand for the cross-sectional average velocity up to the time. However, the sand was divided at 140 seconds and the downstream part was transported as a whole, as seen in Figure 12(b).The rapid change and fluctuation in the sand particle velocity shown in Figure 11 corresponded to the transition of the transport form of the sand. The velocity of the sand particles after 140 seconds, shown as the grey region in Figure 11, represented the cross-sectional and phase-average one. Therefore, this experiment focused on the relation of the sand particle velocity and the seepage force while all of the sand was moving, as indicated by the grey region in Figure 11.

From the measurement of the velocities of the seepage water and the sand particles, the seepage force horizontally exerted on the sand was estimated by the following equation, similar to Eq. (25)

$$f_x = -(1-n)\frac{\partial \overline{p}}{\partial x} + \frac{n^2 \rho_w g}{k}(\tilde{v}_{w,x} - \tilde{v}_{s,x}) \tag{28}$$

where x, f_z, $\tilde{v}_{w,x}$ and $\tilde{v}_{s,x}$ denote the horizontal axis for the macroscopic quantities, the vertical component of the seepage force and the horizontal components of the phase average velocities of the seepage water and the sand particles, respectively. Figure 13 shows the change in the horizontal seepage force, calculated by Eq. (28), during the test. Compared with the results shown in Figure 6, the values of the horizontal seepage force are oscillatory and are not constant. The reason is that the form of the transported sand altered

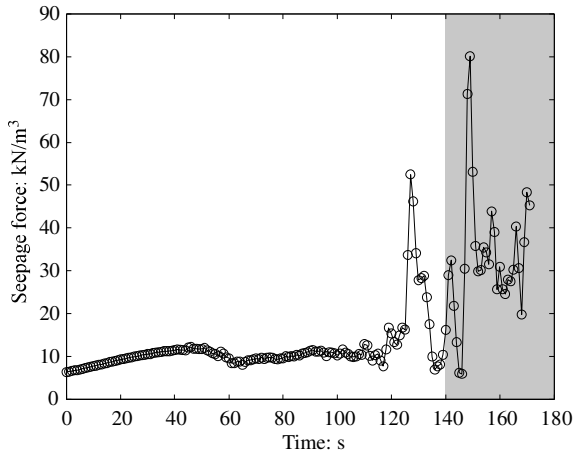

Figure 11 Horizontal velocities of seepage water and sand particles in Test no. H6

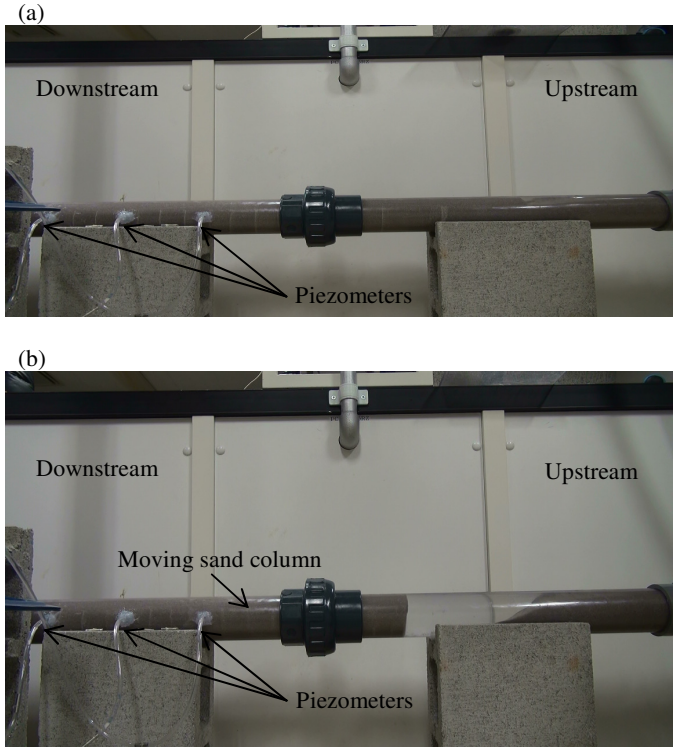

Figure 12 Types of horizontal transportation of sand (Only upper part of sand is moving in (a) and whole left sand column (downstream part) is moving in (b).)

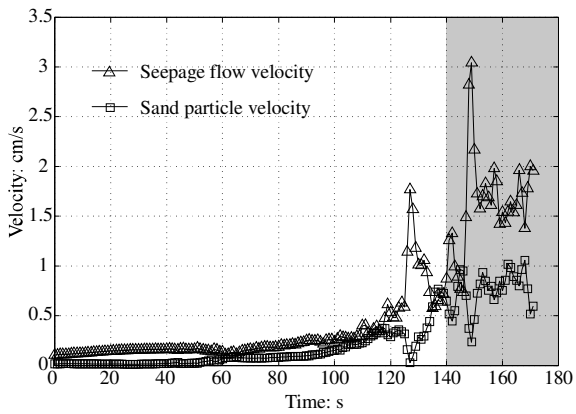

Figure 13 Relationship between seepage force and elapsed time

Table 3 Porosity, density and hydraulic conductivity in sand boil tests with the horizontal pipe

Test no.	Silica sand	Porosity n	Relative density D_r [%]	Temperature T [deg. C]	Hydraulic conductivity k [cm/s]
H1	#5	0.427	87.5	16.0	0.112 (0.109)
H2		0.427	87.5	12.0	0.130 (0.141)
H3		0.433	81.9	16.1	0.134 (0.131)
H4		0.433	81.9	16.0	0.148 (0.145)
H5	#6	0.444	71.3	19.2	0.097 (0.088)
H6		0.431	83.7	17.9	0.074 (0.069)
H7		0.434	80.9	11.6	0.072 (0.078)
H8		0.437	78.1	11.8	0.088 (0.096)

from the partial migration of the particles around the upper part of the pipe to the mass transportation of the sand column. As seen in Figure 13, the fluctuation in seepage force was actually the most intense around 140 seconds, corresponding to the transition point. Moreover, it is worth noting that the values of the seepage force after 140 seconds, when all the sand was moving, were even greater than those shown in Figure 6, which were around 15 kN/m^3. This means that a greater seepage force was needed to convey the sands horizontally than vertically and upward. This fact can explain why the hydraulic gradient decreased in the upward sand boil tests when the sands started to move, because the relatively high hydraulic gradient might have been kept to transport the sands in the horizontal part of the U-shaped cylinder.

Figure 14 shows the relation of the seepage force and the velocity of the sand particles obtained from Test no. H6. When the sand was subjected to the upward seepage flow, the seepage force equilibrated the gravity and the values were almost constant. However, Figure 14 shows the trend whereby the seepage force decreased as the velocity of the sand particles increased when the sand was transported horizontally. Figures 15 and 16 present the relationships between the seepage force and the velocity of the sand particles obtained from Test nos. H1 to H4 and H5 to H8, respectively. Although some variation is exhibited from test to test, the values of the seepage force tend to decrease as the velocity of the sand particles increases. This relation is considered to be natural because the seepage force calculated by Eq. (28) decreases as the velocity of the sand particles increases. Moreover, since the seepage force needed to displace the sand is related to the wall friction of the pipe, the tendency shown in Figures 15 and 16 suggests that the friction may decrease with an increase in the velocity of the sand particles.

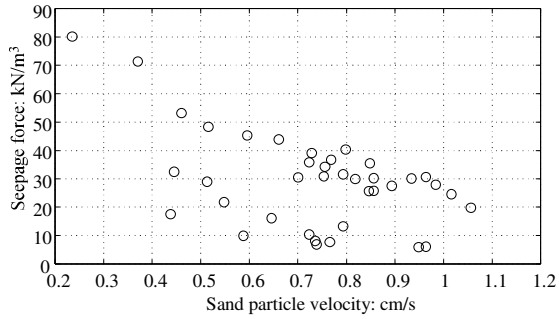

Figure 14 Relation of seepage force and sand particle velocity

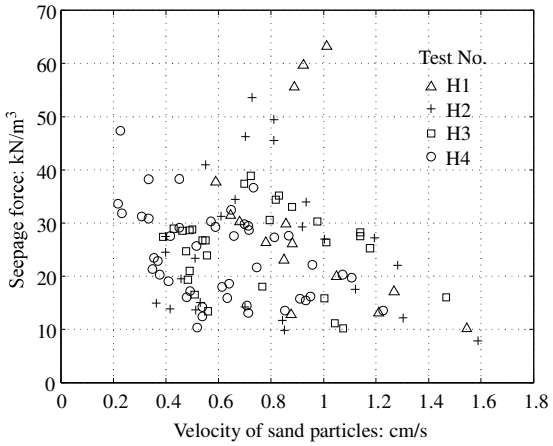

Figure 15 Relationship between velocity of sand particles and seepage force (Silica sand #5)

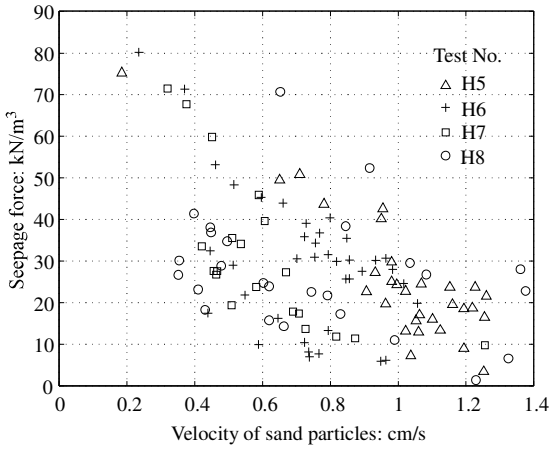

Figure 16 Relationship between velocity of sand particles and seepage force (Silica sand #6)

5. CONCLUSIONS

This paper has explained the seepage force from microscopic and macroscopic points of view and derived Eq. (19) to estimate the seepage force from the macroscopic quantities, such as the phase-averaged water pressure and velocity and the porosity. In the derivation of Eq. (19), the hydraulic conductivity and the phase-averaged seepage water velocity were used to describe the deviation of the microscopic pore water pressure from the macroscopic estimation and the friction between the sand particles and the seepage water. Two types of experiments, using Silica sand #5 and #6 as the test materials, were conducted to investigate the relationship between the seepage force and the velocity of the sand particles transported by the seepage water. One experiment was the sand boil tests by upward seepage flow, and the other examined the horizontal transport of the sands due to the seepage force. In the two experiments, the average velocity of the sand particles, as well as the seepage flow velocity and the hydraulic gradient, were measured from the discharge rates of the sands. The following are the conclusions obtained from the experimental results.

1. During sand boiling induced by upward seepage flow, the seepage force obtained from Eq. (26) was equilibrated with the gravity exerted on the assemblage of the sand particles and kept approximately constant even when the sand particles were moving vertically.
2. The vertical velocity of the sand particles transported by the upward seepage flow was predictable with the aid of the equilibrium equation between the seepage force and the gravity. The prediction of the velocities agreed well with the experimental observations.
3. When the sands were horizontally transported through the entire cross-section of the acrylic pipe, a greater seepage force was needed than that was observed when they moved vertically upward because of the friction between the sand and the pipe walls.
4. The seepage force needed for the horizontal transport of the sand tended to decrease as the velocity of the sand particles increased, which was observed from the repeated test results.

6. ACKNOWLEDGEMENTS

This work was supported by JSPS KAKENHI, Grant-in-Aid for Young Scientists (B), Grant number 23780247.

7. REFERENCES

Foster, M., Fell, R. and Spannagle, M. (2000a) "The statistics of embankment dam failures and accidents". Canadian Geotechnical Journal, 37, pp 1000-1024.

Foster, M., Fell, R. and Spannagle, M. (2000b) "A method for assessing the relative likelihood of failure of embankment dams by piping". Canadian Geotechnical Journal, 37, pp 1025-1061.

Lambe, T.W. and Whitman, R.V. (1979) Soil Mechanics, SI version. John Wiley & Sons, pp 261-264.

Meyer, W., Schuster, R.L. and Sabol, M.A. (1994) "Potential for seepage erosion of landslide dam". Journal of Geotechnical Engineering, 120, Issue 7, pp 1211-1229.

Ojha, C.S.P., Sigh, V.P. and Adrian, D.D. (2003) "Determination of critical head in soil piping". Journal of Hydraulic Engineering, 129, Issue 7, pp 511-518.

Richards, K.S. and Reddy, K.R. (2007) "Critical appraisal of piping phenomenon in earth dams". Bulletin of Engineering Geology and the Environment, 66, pp 381-402.

Richards, K.S. and Reddy, K.R. (2012) "Experimental investigation of initiation of backward erosion piping in soils". Géotechnique, 62, No. 10, pp 933-942.

Sellmeijer, J.B. (1988) "On the mechanism of piping under impervious structures". PhD thesis, Delft University of Technology, the Netherlands.

Sellmeijer, J. B. and Koenders, M. A. (1991) "A mathematical model for piping". Appl. Math. Modelling 15, No. 11–12, pp 646–651.

Shamy, U.EI. and Aydin, F. (2008) "Multiscale modeling of flood-induced piping in river levee". Journal of Geotechnical and Geoenvironmental Engineering, 134, No. 9, pp 1385-1397.

Skempton, A.W. and Brogan, J.M. (1994) "Experiments on piping in sandy gravels". Géotechnique, 44, No. 3, pp 449-460.

Tanaka, T., Kira, H. and Hasegawa, T. (1982) "Design of a loaded filter and multi-layered sand column". Soils and Foundations, 22, No. 3, pp 92-108.

Tanaka, T. and Verruijt A. (1999) "Seepage failure of sand behind sheet piles –The mechanism and practical approach to analyze–". Soils and Foundations, 39, No. 3, pp 27-35.

Zhou, X., Jie, Y., and Li, G. (2012) "Numerical simulation of the developing course of piping". Computers and Geotechnics, 44, pp 104–108.